Inorganic Chemistry
Article

Inorg. Chem. **2009**, *48*, 10679–10686 **10679**
DOI: 10.1021/ic901377h

Planar Hepta-, Octa-, Nona-, and Decacoordinate First Row d-Block Metals Enclosed by Boron Rings

Zhifeng Pu,[†,‡] Keigo Ito,[§] Paul v. R. Schleyer,[*,§] and Qian-Shu Li[*,†,‡]

[†]*School of Chemical Engineering and the Environment, Beijing Institute of Technology, Beijing 100081, China,*
[‡]*Center for Computational Quantum Chemistry, South China Normal University, Guangzhou 510631, China, and*
[§]*Department of Chemistry, Center for Computational Chemistry, University of Georgia, Athens, Georgia 30602*

Received July 14, 2009

Possible planar hypercoordinate molecules with first row d-block metal atoms in the centers of boron rings are explored comprehensively by density-functional theory (DFT) computations. Many optimized MB_n (n = 7, 8, 9, and 10) neutral and charged clusters have local D_{nh} minima, although these may not be the most stable isomers. The larger B_9 and B_{10} rings are versatile in accommodating first row d-block metals, whereas the more compact B_8 ring only can enclose smaller transition metals (such as Mn, Fe, and Co) effectively. Delocalized π and radial molecular orbitals involving boron are crucial in stabilizing these highly symmetrical planar hypercoordinate molecules. Early and middle transition metal d-orbitals participate in metal−boron covalent bonding, whereas partial ionic bonding is more important for the late d-block elements. Potential energy surface scans established several of these species to have planar hypercoordinate global minima: D_{8h} FeB_8^{2-} was identified here, and D_{8h} CoB_8^- and D_{9h} FeB_9^- were identified in an earlier complementary study.

1. Introduction

The field of planar hypercoordinate chemistry continues to expand.[1−6] Understandably, planar hypercoordinate carbon examples have served as the focus of attention[7−23] because drastic deviations from the iconic tetravalent tetrahedral geometries of organic molecules seem so unusual and intriguing. However, planar hypercoordination is by no means limited to carbon. Many molecules containing planar hypercoordinate main group elements, such as boron, nitrogen, oxygen, and heavy metallic elements have been investigated theoretically.[10,24−34] Delocalized bonding involving active

*To whom correspondence should be addressed. E-mail: qsli@bit.edu.cn (Q.S.L.), schleyer@chem.uga.edu (P.v.R.S.).

(1) Sorger, K.; Schleyer, P. v. R. *J. Mol. Struct.* (*THEOCHEM*) **1995**, *338*, 317–346.
(2) Röttger, D.; Erker, G. *Angew. Chem., Int. Ed. Engl.* **1997**, *36*, 812–827.
(3) Siebert, W.; Gunale, A. *Chem. Soc. Rev.* **1999**, *28*, 367–371.
(4) Jemmis, E. D.; Jayasree, E. G.; Parameswara, P. *Chem. Soc. Rev.* **2006**, *35*, 157–168.
(5) Keese, R. *Chem. Rev.* **2006**, *106*, 4787–4808.
(6) Merino, G.; Mendez-Rojas, M. A.; Vela, A.; Heine, T. *J. Comput. Chem.* **2007**, *28*, 362–372.
(7) Exner, K.; Schleyer, P. v. R. *Science* **2000**, *290*, 1937–1940.
(8) Wang, Z.-X.; Schleyer, P. v. R. *Science* **2001**, *292*, 2465–2469.
(9) Wang, Z.-X.; Schleyer, P. v. R. *J. Am. Chem. Soc.* **2001**, *123*, 994–995.
(10) Minyaev, R. M.; Gribanova, T. N.; Starikov, A. G.; Minkin, V. I. *Dokl. Chem.* **2002**, *382*, 41–45.
(11) Wang, Z.-X.; Schleyer, P. v. R. *Angew. Chem., Int. Ed.* **2002**, *41*, 4082–4085.
(12) Li, S.-D.; Miao, C.-Q.; Ren, G.-M. *Eur. J. Inorg. Chem.* **2004**, 2232–2234.
(13) Li, S.-D.; Guo, J.-C.; Miao, C.-Q.; Ren, G.-M. *Angew. Chem., Int. Ed.* **2005**, *44*, 2158–2161.
(14) Li, S.-D.; Miao, C.-Q.; Ren, G.-M.; Guo, J.-C. *Eur. J. Inorg. Chem.* **2006**, 2567–2571.
(15) Li, S.-D.; Miao, C.-Q.; Guo, J.-C. *J. Phys. Chem. A* **2007**, *111*, 12069–12071.
(16) Ito, K.; Chen, Z.; Corminboeuf, C.; Wannere, C.; Zhang, X.-H.; Li, Q.-S.; Schleyer, P. v. R. *J. Am. Chem. Soc.* **2007**, *129*, 1510–1512.
(17) Luo, Q. *Sci. China, Ser. B: Chem.* **2008**, *51*, 1030–1035.
(18) Wu, Y.-B.; Lu, H.-G.; Li, S.-D.; Wang, Z.-X. *J. Phys. Chem. A* **2009**, *113*, 3395–3402.
(19) Averkiev, B. B.; Zubarev, D. Y.; Wang, L.-M.; Huang, W.; Wang, L.-S.; Boldyrev, A. I. *J. Am. Chem. Soc.* **2008**, *130*, 9248–9250.
(20) Boldyrev, A. I.; Simons, J. *J. Am. Chem. Soc.* **1998**, *120*, 7967–7972.
(21) Boldyrev, A. I.; Simons, J.; Li, X.; Wang, L.-S. *J. Chem. Phys.* **1999**, *111*, 4993–4998.
(22) Li, X.; Wang, L.-S.; Boldyrev, A. I.; Simons, J. *J. Am. Chem. Soc.* **1999**, *121*, 6033–6038.
(23) Pei, Y.; An, W.; Ito, K.; Schleyer, P. v. R.; Zeng, X. C. *J. Am. Chem. Soc.* **2008**, *130*, 10394–10400.
(24) Bonačić-Koutecký, V.; Fantucci, P.; Koutecký, J. , *Chem. Rev.* **1991**, *91*, 1035–1108.
(25) Zhai, H.-J.; Alexandrova, A. N.; Birch, K. A.; Boldyrev, A. I.; Wang, L.-S. *Angew. Chem., Int. Ed.* **2003**, *42*, 6004–6008.
(26) Minyaev, R. M.; Gribanova, T. N.; Starikov, A. G.; Minkin, V. I. *Mendeleev Commun.* **2001**, *11*, 213–214.
(27) Li, S.-D.; Miao, C.-Q.; Guo, J.-C.; Ren, G.-M. *J. Am. Chem. Soc.* **2004**, *126*, 16227–16231.
(28) Li, S.-D.; Guo, J.-C.; Miao, C.-Q.; Ren, G.-M. *J. Phys. Chem. A* **2005**, *109*, 4133–4136.
(29) Li, S.-D.; Ren, G.-M.; Miao, C.-Q.; Jin, Z.-H. *Angew. Chem., Int. Ed.* **2004**, *43*, 1371–1373.
(30) Li, S.-D.; Ren, G.-M.; Miao, C.-Q. *Inorg. Chem.* **2004**, *43*, 6331–6333.
(31) Li, S.-D.; Miao, C.-Q. *J. Phys. Chem. A* **2005**, *109*, 7594–7597.
(32) Guo, J.; Yao, W.; Li, Z.; S., L. *Sci. China, Ser. B: Chem.* **2009**, *52*, 566–570.
(33) Miao, C.-Q.; Guo, J.; Li, S. *Sci. China, Ser. B: Chem.* **2009**, *52*, 900–904.
(34) Gribanova, T. N.; Minyaev, R. M.; Minkin, V. I. *Mendeleev Commun.* **2002**, *12*, 170–172.

© 2009 American Chemical Society
Published on Web 10/20/2009

participation of d-orbitals might facilitate planar hypercoordination of transition metal. Although square planar transition metal tetracoordination is well-known,[35] perfectly planar hypercoordination in transition metals (defined as planar coordination higher than four for transition metals) is unknown experimentally. The hexacoordinate nickel atom in the tribenzocyclyne nickel(0) complex (Ni(TBC)),[36] is located ~0.3 Å above the ring plane; the $SiPh_2$- and $GePh_2$ substituted derivatives of Ni(TBC) also have near-planar local Ni geometries.[37−39] The Mn_5 unit in Schollenberger et al.'s $[In(Mn(CO)_4)_5]^{2-}$ potassium salt coordinates to the In atom, but has an envelope-shape.[40] $[Ni(t\text{Bu-P})_6]$ contains a quasi-planar cyclic P_6 moiety enveloping a $16e^-$ nickel atom.[41] Remarkably, Tang, Hoffman, Albright, Deng, and Hoffmann's[42] computational survey of this species and its relatives showed that planar saturated group 14 rings were capable of binding transition metal atoms in their centers quite strongly.

Other theoretical explorations have had limited success. Although Massobrio et al. computed the first example of a perfectly planar pentacoordinate hexatomic cluster isomer, Cu_6 (C_{2v}), this was not the global minimum and its central Cu atom was surrounded by an irregular Cu_5 pentagon (shaped like a baseball home plate). A three-dimensional C_{2v} Cu_6 cluster was 7.8 kcal/mol lower in energy.[43] Häkkinen and Landman identified a planar gold cluster, Au_7 (D_{2h}), with a hexacoordinate gold atom at the center of an Au_6 ring.[44] Frenking and co-workers characterized singlet D_{5h} $FeBi_5^+$ and $FeSb_5^+$ as planar minima theoretically; however, the non-planar triplet states of these species were more stable.[45]

Boldyrev has emphasized the usefulness of boron ring perimeters to promote planar hypercoordination of enclosed elements.[19,25,46−51] Boron, because of its electron deficiency and proclivity for deltahedral bonding, is the "planar element" par excellence, and facilitates the planar hypercoordination of carbon[7,8,24,52−62] Indeed, examples of boron cluster−containing first row transition metals were identified as global and local minima recently.[63−67] Our earlier investigation, complementary to the present work, focused on two anionic global minima, D_{8h} CoB_8^- and D_{9h} FeB_9^-.[68] However, there has been no prior systematic study of planar cyclic boron clusters encapsulating transition metals. Hence, the goal of the present paper is to elucidate the periodic trends of the stability, geometry, bonding, and magnetic aromaticity of such hypercoordinate transition metal clusters. We predict that first row d-block atoms (M) can form numerous planar MB_n species with M in the center of planar *n*-membered boron rings B_n (n = 7 to 10). The Schleyer−Boldyrev[69] design principles for planar hypercoordination stress the need for both optimum electronic and geometrical "fit." To satisfy the geometric fit, the boron ring sizes were varied from seven- to ten-membered to encapsulate the first row d-block metals with different atomic sizes. In addition, molecular charges were chosen so that degenerate highest molecular orbitals were fully occupied to avoid Jahn−Teller distortion.

2. Theoretical Methods

All geometries were optimized at the B3LYP[70,71]/6-311 + G*[72,73] level of theory, employing Gaussian 03.[74] Harmonic vibrational frequencies were computed at the same level to characterize the nature of the stationary points. Total energies were corrected by the unscaled zero-point energies (ZPE). Natural bond orbital (NBO)[75] analyses at

(35) Cotton, F. A.; Wilkinson, G.; Murillo, C. A.; Bochmann, M. *Advanced Inorganic Chemistry*, 6th ed.; Wiley: New York, 1999.
(36) Ferrara, J. D.; Tanaka, A. A.; Fierro, C.; Tesssier-Youngs, C. A.; Youngs, W. J. *Organometallics* **1989**, *8*, 2089–2098.
(37) Guo, L.; Bradshaw, J. D.; Tessier, C. A.; Youngs, W. J. *Organometallics* **1995**, *14*, 586–588.
(38) Guo, L.; Bradshaw, J. D.; McConville, D. B.; Tessier, C. A.; Youngs, W. J. *Organometallics* **1997**, *16*, 1685–1692.
(39) Youngs, W. J.; Tessier, C. A.; Brandsaw, J. D. *Chem. Rev*. **1999**, *99*, 3153–3180.
(40) Schollenberger, M.; Nuber, B.; Ziegler, M. *Angew. Chem., Int. Ed. Engl*. **1992**, *31*, 350–351.
(41) Ahlrichs, R.; Fenske, D.; Oesen, H.; Schneider, U. *Angew. Chem., Int. Ed. Engl*. **1992**, *31*, 323–326.
(42) Tang, H.; Hoffman, D.; Albright, T. A.; Deng, H.; Hoffmann, R. *Angew. Chem., Int. Ed. Engl*. **1993**, *32*, 1616–1618.
(43) Massobrio, C.; Pasquarello, A.; Corso, A. D. *J. Chem. Phys*. **1998**, *109*, 6626–6630.
(44) Häkkinen, H.; Landman, U. *Phys. Rev. B* **2000**, *62*, R2287–R2290.
(45) Lein, M.; Frunzke, J.; Frenking, G. *Angew. Chem., Int. Ed*. **2003**, *42*, 1303–1306.
(46) Zubarev, D. Y.; Boldyrev, A. I. *J. Comput. Chem*. **2007**, *28*, 251–268.
(47) Wang, L. M.; Huang, W.; Averkiev, B. B.; Boldyrev, A. I.; Wang, L.-S. *Angew. Chem., Int. Ed*. **2007**, *46*, 4550–4553.
(48) Averkiev, B. B.; Boldyrev, A. I. *Russ. J. Gen. Chem*. **2008**, *78*, 769–773.
(49) Alexandrova, A. N.; Boldyrev, A. I.; Zhai, H.-J.; Wang, L.-S.; Steiner, E.; Fowler, P. W. *J. Phys. Chem. A* **2003**, *107*, 1359–1369.
(50) Alexandrova, A. N.; Boldyrev, A. I.; Zhai, H.-J.; Wang, L.-S. *J. Phys. Chem. A* **2004**, *108*, 3509–3517.
(51) Alexandrova, A. N.; Zhai, H.-J.; Wang, L.-S.; Boldyrev, A. I. *Inorg. Chem*. **2004**, *43*, 3552–3554.
(52) Kato, H.; Yamashita, K. *Chem. Phys. Lett*. **1992**, *190*, 361–366.
(53) Kato, H.; Yamashita, K.; Morokuma, K. *Bull. Chem. Soc. Jpn*. **1993**, *1993*, 3358–3361.
(54) Boustani, I. *Int. J. Quantum Chem*. **1994**, *52*, 1081–1111.
(55) Ricca, A.; Bauschlicher, C. W. *J., Chem. Phys*. **1996**, *208*, 233–242.
(56) Gu, F. L.; Yang, X.; Tang, A.-C.; Jiao, H.; Schleyer, P. v. R. *J. Comput. Chem*. **1998**, *19*, 203–214.
(57) Gribanova, T. N.; M., M. R.; Minkin, V. I. *Russ. J. Inorg. Chem*. (*Engl. Transl*.) **2001**, *46*, 1340–1343.
(58) Gribanova, T. N.; Minyaev, R. M.; Minkin, V. I. *Mendeleev Commun*. **2001**, 169–170.
(59) Jin, H. W.; Li, Q. S. *Phys. Chem. Chem. Phys*. **2003**, *5*, 1110–1115.
(60) Li, Q.; Zhao, Y.; Xu, W.; Li, N. *Int. J. Quantum Chem*. **2004**, *101*, 219–229.
(61) Aihara, J.-I.; Kanno, H.; Ishida, T. *J. Am. Chem. Soc*. **2005**, *127*, 13324–13330.
(62) Yu, H.-L.; Sang, R.-L.; Wu, Y.-Y. *J. Phys. Chem. A* **2009**, *113*, 3382–3386.
(63) Liu, X. L.; Zhao, G.-F.; Guo, L.-J.; Jing, Q.; Luo, Y.-H. *Phys. Rev. A* **2007**, *75*, 063201-1-6.
(64) Yang, Z.; Xiong, S.-J. *J. Chem. Phys*. **2008**, *128*, 184310−1–184310−8.
(65) Yao, J.-G.; Wang, X.-W.; Wang, Y.-X. *Chem. Phys*. **2008**, *351*, 1–6.
(66) Luo, Q. *Sci. China, Ser. B: Chem*. **2008**, *51*, 607–613.
(67) Wu, Q.; Tang, Y.; Zhang, X. *Sci. China, Ser. B: Chem*. **2009**, *52*, 288–294.
(68) Ito, K.; Pu, Z.; Li, Q.-S.; Schleyer, P. v. R. *Inorg. Chem*. **2008**, *47*, 10906–10910.
(69) Schleyer, P. v. R.; Boldyrev, A. I. *J. Chem. Soc., Chem. Commun*. **1991**, 1536–1538.
(70) Becke, A. D. *J. Chem. Phys*. **1993**, *98*, 5648–5652.
(71) Lee, C.; Yang, W.; Parr, R. G. *Phys. Rev. B* **1988**, *37*, 785–789.
(72) Studies by Jensen, et al. and Riley and Merz show that the B3LYP functional performed relatively well in predicting bond distances, partial charges, and ionization potentials for molecules containing the first row transition metals. For details, see: (a) Jensen, K. P.; Roos, B. O.; Ryde, U. *J. Chem. Phys*. **2007**, *126*, 014103−1–014103−14. (b) Riley, K. E.; Merz, K. M., Jr. *J. Phys. Chem. A* **2007**, *111*, 6044–6053.
(73) An artifact imaginary frequency in a planar hypercoordinate carbon, D_{6h} CB_6^{2-}, at MP2/6-311+G* level was reported by Shahbazian (see: Shahbazian, S. *Chem. Phys. Lett*. **2007**, *443*, 147–151). However, we did not observe any inconsistencies in the total energies and harmonic vibrational frequencies between B3LYP/6-311+G* and B3LYP/def2-TZVPP, a larger and more accurate basis set (See Supporting Information, Table S4).
(74) Frisch, M. J. et al. *Gaussian 03*, Revision C.02; Gaussian, Inc.: Wallingford, CT, 2004.
(75) Glendening, E. D.; Badenhoop, J. K.; Reed, A. E.; Carpenter, J. E.; Bohmann, J. A.; Morales, C. M.; Weinhold, F. *NBO*, 5.G; University of Wisconsin: Madison, WI, 2001.

B3LYP/6-311G* provided insight into the bonding. Out-of-plane nucleus-independent chemical shifts at points 1.0 Å above the boron ring centers (NICS(1))[76,77] were computed at the GIAO[78,79]/B3LYP/6-311G* level. A grid of $NICS_{zz}$ points, similar to the induced magnetic field analysis,[80] was performed at the same level, at 1.0 Å spacings. The potential energy surface of FeB_8^{2-} was scanned using "Kick", a stochastic search method.[81,82] A total of 10500 structures with singlet, triplet, and quintuplet states were initially optimized at HF/STO-3G level. Further geometric and energetic refinement were carried out at B3LYP/6-311+G*.

3. Results and Discussion

Our theoretical survey predicts many neutral and charged MB_n (n = 7 to 10) singlet, doublet, triplet, and quintuplet minima with planar D_{nh} (n = 7 to 10) symmetries. Table 1 summarizes the computed zero-point energies, the lowest vibrational frequencies, the highest occupied molecular orbital (HOMO)−lowest unoccupied molecular orbital (LUMO) gaps, and the bond lengths of the singlet planar hypercoordinate metal (phM) minima. The lowest vibrational frequencies of the singlet phMs are generally appreciable, indicating geometrical stability. The smallest positive vibrational frequency of D_{10h} NiB_{10}^{2+} is rather low (26.8 cm^{-1}, see Table1); however, the vibrational trajectory confirms that the planar geometry of the NiB_{10}^{2+} is indeed a minimum (see Supporting Information, Figure S1). The HOMO−LUMO gaps of the singlet phM species are ample (ranging from 1.46 in CuB_{10}^{3+} to 3.35 eV in ZnB_9^-) (see Table 1, Gap), except for D_{9h} TiB_9^{3-} (0.67 eV) and D_{10h} ScB_{10}^{3-} (0.61 eV). However, no instabilities in the electron density were found in any of the phM species reported here. Tables S1 to S3 provided in the Supporting Information summarize the data for the doublet, triplet, and quintuplet minima.

Ring Size Effect on Stability. The seven-membered boron ring (7MR) is too small to encapsulate the relatively large d-block metals. Only singlet D_{7h} CoB_7^{2+} was identified as a 7MR minimum. The Co−B bond distance (1.901 Å) is significantly shorter than the sum of covalent radii of the Co and B atoms[83] (2.10 Å; see Table 4), and results in a significant steric repulsion between Co and the B_7 ring. The B−B bond distance (1.649 Å) is significantly longer than typical B−B bond distances (ranging from 1.529 to 1.593 Å) reported in the D_{nh} AB_n (A = Group 14 elements).[84] This suggests steric repulsion between the B_7 ring moiety and the central cobalt. The B_7 ring expands (but not enough to rupture) to accommodate the large cobalt atom at the center.

Table 1. Zero-Point Energies (ZPE, kcal/mol), Lowest Vibrational Frequencies (ν_{min}, cm^{-1}), HOMO−LUMO Gap (Gap, eV), M−B and B−B Bond Lengths (R_{M-B} and R_{B-B}, Å) of the Singlet Structures Computed at B3LYP/6-311+G*

	ZPE	ν_{min}	Gap	R_{M-B}	R_{B-B}
CoB_7^{2+}	16.2	99.1	1.92	1.901	1.649
MnB_8^{3+}	18.3	100.0	2.12	2.090	1.599
CoB_8^{3+}	17.9	176.9	1.78	2.093	1.602
FeB_8^{2-}	20.3	90.7	2.51	2.043	1.563
CoB_8^-	20.4	59.2	2.73	2.036	1.559
TiB_9^{3-}	22.0	117.8	0.67	2.292	1.568
VB_9^{2-}	22.7	139.5	2.37	2.252	1.541
CrB_9^-	22.7	132.4	2.18	2.232	1.527
MnB_9	22.1	92.0	1.77	2.231	1.526
MnB_9^{2-}	22.4	128.6	2.91	2.232	1.527
FeB_9^-	22.4	110.5	3.08	2.220	1.519
CoB_9	22.0	96.7	2.47	2.226	1.522
NiB_9^+	21.4	110.5	1.99	2.251	1.540
CuB_9^{2-}	21.5	116.5	2.28	2.258	1.545
ZnB_9^-	22.0	83.7	3.35	2.264	1.549
ScB_{10}^{3-}	23.9	134.7	0.61	2.516	1.555
TiB_{10}^{2-}	24.5	118.2	2.35	2.468	1.525
VB_{10}^-	24.3	71.5	2.26	2.442	1.509
FeB_{10}^{2+}	21.9	63.8	1.71	2.489	1.538
NiB_{10}^{2+}	21.8	26.8	1.73	2.492	1.540
CuB_{10}^{3+}	21.5	72.8	1.46	2.551	1.577
CuB_{10}^-	23.3	112.3	2.77	2.465	1.524
ZnB_{10}	23.6	114.6	2.99	2.476	1.530

Table 2. NPA Charges of the M Atoms (Charge), Wiberg Bond Indices of M−B (WBI_{M-B}), and Total Wiberg Bond Indices of the Transition Metal M (WBI_M) of the Singlet Structures Computed at B3LYP/6-311G*

	charge	WBI_{M-B}	WBI_M
CoB_7^{2+}	0.258	0.40	2.77
MnB_8^{3+}	0.536	0.48	3.75
CoB_8^{3+}	0.504	0.36	2.86
FeB_8^{2-}	0.770	0.45	3.56
CoB_8^-	0.112	0.36	2.88
TiB_9^{3-}	1.082	0.49	4.43
VB_9^{2-}	1.114	0.52	4.61
CrB_9^-	1.115	0.56	4.52
MnB_9	1.179	0.41	3.54
MnB_9^2	1.019	0.44	3.90
FeB_9^-	1.031	0.39	3.53
CoB_9	1.024	0.32	2.89
NiB_9^+	1.043	0.23	2.05
CuB_9^{2-}	1.231	0.11	1.00
ZnB_9^-	1.742	0.10	0.87
ScB_{10}^{3-}	1.361	0.29	2.89
TiB_{10}^{2-}	1.399	0.48	4.34
VB_{10}^-	1.376	0.46	4.51
FeB_{10}^{2+}	1.233	0.26	2.49
NiB_{10}^{2+}	1.086	0.20	2.01
CuB_{10}^{3+}	0.903	0.12	1.18
CuB_{10}^-	1.210	0.10	0.91
ZnB_{10}	1.655	0.10	0.92

Unlike the B_7 moiety, the ring cavity size in the eight-membered ring (8MR) is large enough to accommodate the small d-block metals. Four singlet minima, D_{8h} MnB_8^{3+}, CoB_8^{3+}, FeB_8^{2-}, and CoB_8^-, were identified. Six other minima with doublet, triplet and quintuplet states are summarized in the Supporting Information (see Tables S1 to S3). The M−B bond distances of D_{8h} MnB_8^{3+} and FeB_8^{2-} (2.090 and 2.043 Å, respectively;

(76) Schleyer, P. v. R.; Maerker, C.; Dransfeld, A.; Jiao, H.; Hommes, N. J. R. v. E. *J. Am. Chem. Soc.* **1996**, *118*, 6317–6318.
(77) Schleyer, P. v. R.; Jiao, H.; Hommes, N. J. R. v. E.; Malkin, V. G.; Malkina, O. L. *J. Am. Chem. Soc.* **1997**, *119*, 12669–12670.
(78) Dodds, J. L.; McWeeny, R.; Sadlej, A. J. *Mol. Phys.* **1980**, *41*, 1419–1430.
(79) Wolinski, K.; Hilton, J. F.; Pulay, P. *J. Am. Chem. Soc.* **1990**, *112*, 8251–8260.
(80) Merino, G.; Heine, T.; Seifert, G. *Chem.—Eur. J.* **2004**, *10*, 4367–4371.
(81) Saunders, M. *J. Am. Chem. Soc.* **1987**, *109*, 3150–3152.
(82) Bera, P. P.; Sattelmeyer, K. W.; Saunders, M.; Schaefer, H. F., III.; Schleyer, P. v. R. *J. Phys. Chem. A* **2006**, *110*, 4287–4290.
(83) Cordero, B.; Gómez, V.; Platero-Prats, A. E.; Revés, M.; Echeverría, J.; Cremades, E.; Barragán, F.; Alvarez, S. *Dalton Trans.* **2008**, 2832–2838.
(84) Islas, R.; Heine, T.; Ito, K.; Schleyer, P. v. R.; Merino, G. *J. Am. Chem. Soc.* **2007**, *129*, 14767–14774.

Table 3. NICS(1)$_{zz}$ Values (ppm), and the Number of π, Radial, d Lone Pair, σ, and Total Valence Electrons (N_π, N_{Rad}, N_{dlp}, N_σ, N_{Tot}) of Singlet Structures Computed at B3LYP/6-311G*

	NICS(1)$_{zz}$	N_π	N_{Rad}	N_{dlp}	N_σ	N_{Tot}
CoB_7^{2+}	−77.6	6	2	6	14	28
MnB_8^{3+}	−71.2	6	6	0	16	28
CoB_8^{3+}	−75.4	6	6	2	16	30
FeB_8^{2-}	−87.0	6	10	2	16	34
CoB_8^{-}	−90.8	6	10	2	16	34
TiB_9^{3-}	−76.7	6	10	0	18	34
VB_9^{2-}	−80.1	6	10	0	18	34
CrB_9^{-}	−84.5	6	10	0	18	34
MnB_9	−87.2	6	10	0	18	34
MnB_9^{2-}	−90.6	6	10	2	18	36
FeB_9^{-}	−93.0	6	10	2	18	36
CoB_9	−91.4	6	10	2	18	36
NiB_9^{+}	−89.9	2	10	6	18	36
CuB_9^{2-}	−102.9	6	6	10	18	40
ZnB_9^{-}	−95.7	6	6	10	18	40
ScB_{10}^{3-}	−85.0	6	10	0	20	36
TiB_{10}^{2-}	−83.3	6	10	0	20	36
VB_{10}^{-}	−85.2	6	10	0	20	36
FeB_{10}^{2+}	−84.5	2	10	4	20	36
NiB_{10}^{2+}	−83.5	2	8	8	20	38
CuB_{10}^{3+}	−81.1	2	6	10	20	38
CuB_{10}^{-}	−100.5	6	6	10	20	42
ZnB_{10}	−93.3	6	10	6	20	42

Table 4. Sum of M−B Covalent Radii,* and B−B Double Bond Covalent Bond Distances[a] ($R_{Ref.}$) in Å[b]

Bond	$R_{Ref.}$[b]
Sc−B	2.54
Ti−B	2.44
V−B	2.37
Cr−B	2.23
Mn−B (l.s.)[b]	2.23
Mn−B (h.s.)[b]	2.45
Fe−B (l.s.)[b]	2.16
Fe−B (h.s.)[b]	2.36
Co−B (l.s.)[b]	2.10
Co−B (h.s.)[b]	2.34
Ni−B	2.08
Cu−B	2.16
Zn−B	2.06
B=B	1.561

[a] The B=B bond distance was taken from ref 85. [b] For Mn, Fe, and Co, low- and high-spin are indicated by l.s. and h.s., respectively. Covalent radii and spin state designations were taken from ref 83.

see Table 1) are substantially shorter than their covalent radii sums (2.23 and 2.36 Å, respectively; see Table 4);[83] this suggests that weak steric repulsions between the central metal atom and the cyclic boron ligand may exist. On the other hand, the M−B bond distances of D_{8h} CoB_8^{3+} and CoB_8^{-} (2.093 and 2.036 Å, respectively; see Table1) are comparable to the sum of M−B covalent radii (2.10 Å, see Table 4),[83] indicating that the atomic size of cobalt is a good match for the B_8 ring cavity. The optimal Co−B bond distances should result in strong interactions between the cobalt and the boron ring without causing significant steric repulsions. The B−B bond lengths in D_{8h} MnB_8^{3+}, CoB_8^{3+}, FeB_8^{2-}, and CoB_8^{-} (1.599, 1.602, 1.563, and 1.559 Å, respectively, see Table 1) are much shorter than that in CoB_7^{2+} (1.649 Å) but are very similar to the experimentally detected B=B bond distance (1.560 Å),[85] which suggest the diminished steric effects in the 8MR species because of the enlarged ring cavity.

Nine-membered rings (9MR) appear to be more suitable than 7MR or 8MR for encapsulating the first row d-block metals. There are 10 singlet planar nonacoordinate minima (see Table 1) and 11 other minima with higher spin states (see Supporting Information, Tables S1 to S3). The early d-block metals are slightly too small for optimum binding by the B_9 ring ligand. The Ti−B and V−B bond distances in the D_{9h} TiB_9^{3-} and VB_9^{2-} (2.292 and 2.252 Å, respectively; see Table 1) are slightly shorter than the sums of their covalent radii[83] (2.44 and 2.37 Å, respectively; see Table 4), while the B−B bond distances are similar to that of B=B (1.560 Å).[85] Such short M−B and B−B bond distances indicate that there are mainly bonding interactions between the central metal atoms and the boron ring moiety, but no appreciable steric repulsions exist. Middle d-block elements, such as Cr and Mn, provide the best geometric matches with a B_9 ring. The M−B bond distances in the D_{9h} CrB_9^{-}, MnB_9, and MnB_9^{2-} (2.232, 2.231, and 2.232 Å, respectively) are almost identical to the sums of the covalent bond distances (2.23 Å for both Cr−B and Mn−B, see Table 4). Such good matches between the B_9 ring and Cr and Mn should increase the stability of CrB_9^{-} and MnB_9, according to Schleyer−Boldyrev rules.[69] The remaining singlet MB_9 minima, mainly consisting of the late d-block metals, such as FeB_9^{-}, CoB_9, NiB_9^{+}, CuB_9^{2-}, and ZnB_9^{-}, have slightly longer M−B bond distances (2.220, 2.226, 2.251, 2.258, and 2.264 Å, respectively)(see Table 1) than the sums of the covalent distances (2.16, 2.10, 2.08, 2.16, and 2.06 Å, respectively; see Table 4). Although the poorer "fit" diminishes the strength of individual M−B bonding interactions, this disadvantage is overcome by the unusually large number of M−B bonds.

The cavity size of the B_{10} ligand is much greater than the metal covalent radii in the singlet ten-membered ring (10MR) systems.[83] Only metals with large radii, such as Sc and Ti, can interact with the large B_{10} ligand satisfactorily. The M−B bond distances in D_{10h} ScB_{10}^{3-} and TiB_{10}^{2-}, 2.516 and 2.468 Å, respectively, are similar to the covalent radii sums of the metal and boron atom (2.54 and 2.44 Å, respectively; see Table 4). Hence, Sc and Ti atoms are good matches for the 10MR boron ring. In the remaining singlet 10MR phM minima (see Table 1), the M−B bonding interactions are weaker than the 7MR, 8MR, or the 9MR systems because of the larger M−B separations. Nonetheless, overall stability is achieved since the large number of M−B interactions makes up for the individual weakness of each one.

M−B Interaction Across the d-Block. Molecular orbital (MO) analyses of D_{10h} VB_{10}^{-}, D_{9h} FeB_9^{-}, and ZnB_9^{-} elucidate the M−B interactions of phM anions containing early, middle, and late transition metals, respectively. The MOs of VB_{10}^{-} show that the vanadium d orbitals participate actively in the bonding (see Figure 1). The in-plane d_{xy} and $d_{x^2-y^2}$ vanadium atomic orbitals (AOs) interact favorably with the degenerate radial MOs with

(85) Wang, Y.; Quillian, B.; Wei, P.; Wannere, C. S.; Xie, Y.; King, R. B.; Schaefer, H. F., III.; Schleyer, P. v. R.; Robinson, G. H. *J. Am. Chem. Soc.* **2007**, *129*, 12412–12413.

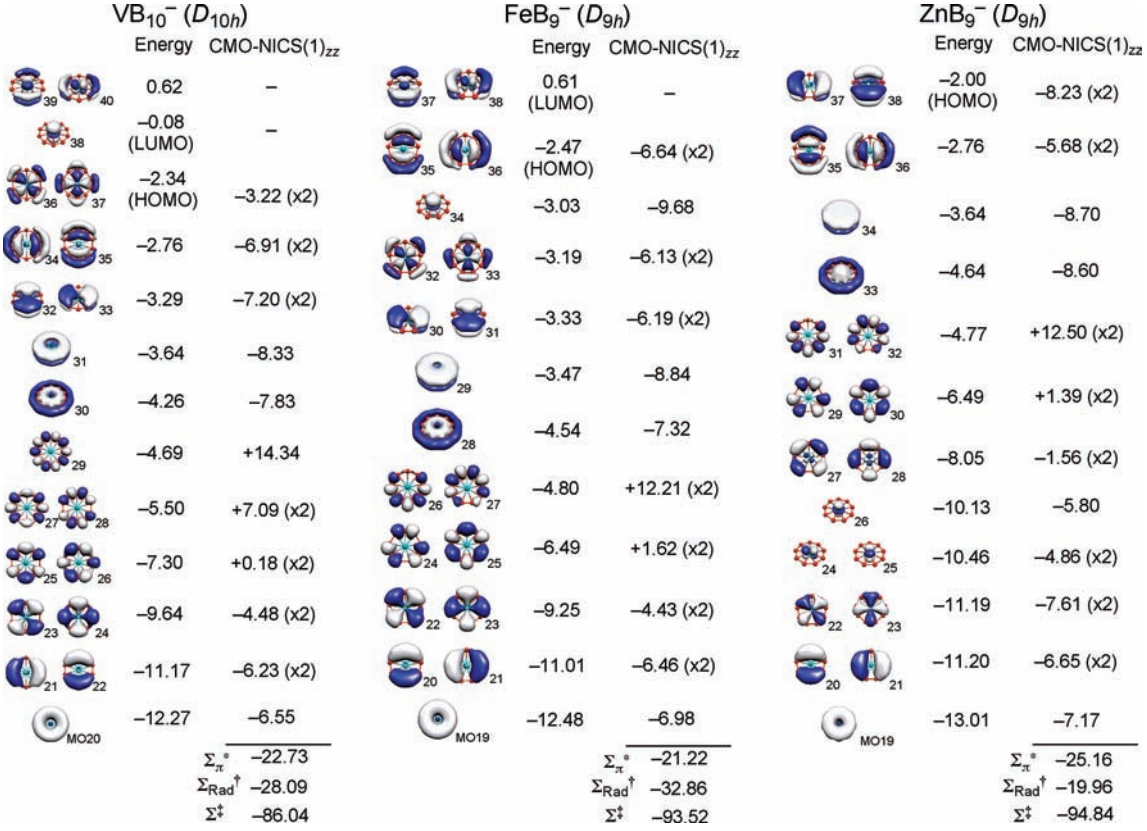

Figure 1. MOs of D_{10h} VB_{10}^-, D_{9h} FeB_9^-, and D_{9h} ZnB_9^- (at B3LYP/6-311+G*; energies in eV) and their CMO-NICS(1)$_{zz}$ contributions (in ppm) at B3LYP/6-311G*. *The sum of NICS tensor contributions from the π MOs ($\sum\pi$) includes MOs 31, 32, and 33 for VB_{10}^-, MOs 29, 30, and 31 for FeB_9^-, and MOs 34, 37, and 38 for ZnB_9^-. †The sum of NICS tensor contributions from the radial MOs ($\sum_{Rad}$) includes MOs 30, 34−37 for VB_{10}^-, MOs, 28, 32,33,35 and 36 for FeB_9^-, and MOs 33, 35, and 36 for ZnB_9^-. ‡The sum of NICS tensor contributions from all other MOs ($\sum$) include core and σ MOs.

two nodes (rad_2) (radial MOs are delocalized, in-plane MOs composed of boron $p_{(x,y)}$ AOs pointing at the center of the ring), resulting in the degenerate HOMOs (MO 36 and 37). The interaction of the lowest radial MO (rad_0) with the vanadium s AO results in MO 30. Although the $3d_{z^2}$ AO can hybridize with the 4s AO to some degree, such mixing is evidently small. The d_{z^2} (MO 38) is part of the LUMO. Hence, the rad_0 and rad_2 MOs not only help to bind peripheral boron atoms, but also fuse the vanadium atom to the boron ring. On the other hand, a degenerate pair of radial MOs with one node (rad_1) have the correct symmetry to interact with the vanadium $p_{(x,y)}$ AO; however, the vanadium p AO energies are too low to interact with the B_{10} rad_1 MOs; the resulting MOs 34 and 35 mostly participate in boron ring radial bonding; the M−B bonding is negligible. There are 10 radial electrons; hence VB_{10}^- is expected to have radial aromaticity.[86] In addition to the strong radial bonding interaction between the vanadium and the boron ring, the vanadium $d_{(xz,yz)}$ AOs further contribute to the stability of VB_{10}^- via d-π interactions, as depicted in MOs 32 and 33. A similar d-π interaction was reported in D_{5h} $FeSb_5^+$ and $FeBi_5^+$ by Frenking et al.[45] The lowest π MO (MO 31) binds the peripheral boron atoms of VB_{10}^- together efficiently, but it does not contribute to the V−B bonding significantly. The energy of the vanadium p_z AO is too low to interact effectively with the boron ring π MO. VB_{10}^- is π-aromatic since its 6 π electrons satisfy the Hückel rule. Overall, VB_{10}^- is a 16-e$^-$ TM species (counting the six electrons in the vanadium p AOs (not shown in Figure 1), together with MOs 30, 32, 33, 36 and 37); the d_{z^2} (MO 38) remains vacant. With the exception of the occupied d_{z^2} AO (MO 34), the electronic structure of D_{9h} FeB_9^- is similar to that of D_{10h} VB_{10}^-. Hence, FeB_9^- satisfies the 18-electron rule. The MOs of FeB_9^- clearly show that the 6 π and 10 radial electron counts maximize both the M−B and the B−B bonding in the phM species containing early to middle d-block elements. Additional electrons would be unfavorable as they would have to occupy antibonding d-π MOs.

In contrast, the bonding pattern of D_{9h} ZnB_9^- is quite different from D_{10h} VB_{10}^- and D_{9h} FeB_9^- since all the d AOs of zinc are occupied and do not participate in Zn−B bonding. The non-bonding $d_{(xz,yz)}$ and d_{z^2} (MOs 24−26) are shown in Figure 1. ZnB_9^- has six π electrons (MOs 34, 37, and 38) but only six radial electrons (MOs 33, 35, and 36; note that both VB_{10}^- and FeB_9^- have ten radial e$^-$'s). Only rad_0 MO 33 binds the central zinc atom of ZnB_9^- with the boron ring moiety; the remaining MOs contribute to the B−B bonding. Furthermore, the HOMOs have slight antibonding character between zinc and the boron ring. Hence, the planarity of ZnB_9^- must be due mainly to the boron ring π and radial bonding, although partial ionic interactions between the positively charged Zn and the negatively charged B_9 ring (see Natural Population Analysis (NPA) Charge section) also contribute.

(86) Chandrasekhar, J.; Jemmis, E. D.; Schleyer, P. v. R. *Tetrahedron Lett.* **1979**, *39*, 3707–3710.

Wiberg Bond Index Analyses. The computed individual M−B Wiberg bond indexes (WBI_{M-B}) of the singlet phMs and the sum of the Wiberg bond indices of the metal centers (WBI_M) are tabulated in Table 2. The individual M−B bonding interactions are weaker than a single M−B bond for all species listed, but such weak interactions are compensated by the large number of M−B interactions. The WBI_{M-B}'s in the 7MR and 8MR species are small (ranging from 0.36 to 0.48), but the WBI_M sums (ranging from 2.86 to 3.75) document the significant total covalent bonding between the central metal and the peripheral boron rings. The WBI_{M-B} values of TiB_9^{3-}, VB_9^{2-}, CrB_9^-, MnB_9, and MnB_9^{2-} (ranging from 0.41 to 0.56) (Table 2) document the moderate covalent bonding between the central metal and the individual boron atoms. In contrast, the smaller WBI_{M-B}'s of the late transition metal elements indicate diminished covalent interactions, as discussed in the MO interaction section. The WBI_{M-B} of D_{9h} NiB_9^+, CuB_9^{2-}, and ZnB_9^-, 0.23, 0.11, and 0.10, respectively, reflect the inherently weak covalent bonding character of late d-block metals because of the reduced participation of their d AOs. The covalent interactions between the central atoms and the larger 10 membered boron ring are smaller. The middle transition metals are too small to fit into the B_{10} ring cavity; hence their WBI_{M-B} values are small. Nonetheless, relatively large, early d-block elements, such as Ti and V, can interact strongly with the B_{10} ligand; TiB_{10}^{2-} and VB_{10} have high WBI_{M-B} values (0.48 and 0.46, respectively). Furthermore, the d AOs in the late metals are essentially inert, resulting in very small WBI_{M-B} values. This is consistent with the MO analysis.

NPA Charges. All metal atom charges of the central d-block metals in the singlet phM minima are positive (Table 2). According to the Allred−Rochow electronegativity scale,[87] the electronegativity of boron (2.01) is higher than any of the first row d-block elements (which range from 1.20 to 1.75). The resulting partial ionic M−B bonding character increases the stability of the phMs. Such partial ionic bonding is especially important for phM minima with late d-block elements, where the M−B covalent bonding is reduced because of the inactivity of the d AOs. In particular, the partial charges of the Zn atom in D_{9h} ZnB_9^- and D_{10h} ZnB_{10} are +1.742 and +1.655, while the partial boron atom charges are −0.305 and −0.170, respectively.

Metal−Ligand Binding Energies. Vertical metal−ligand binding energies of the central metal to the boron ring ligand ($M-B_n$) for D_{9h} MnB_9, CoB_9, and D_{10h} ZnB_{10} (6.43, 6.91, and 4.86 eV, respectively) (see Table 5 for details) document the strong M−B interactions, which are due to the effective use of the metal d AOs and the partial ionic character of the $M-B_n$ bonds. The $M-B_n$ binding energy of Zn is significantly smaller than that of Mn and Co because of diminished Zn−B covalent bond character and the larger Zn−B separation due to the greater boron ring diameter. Despite this less favorable bonding situation, the binding energy of ZnB_{10} is still very large; this demonstrates the significance of ionic bonding in phM.

Table 5. Total Energies ($E_{Tot.}$, a.u.) of D_{9h} MnB_9, CoB_9 and D_{10h} ZnB_{10}, and Its Fragments, and the Vertical Metal-Ligand Binding Energies (BE, eV) Computed at B3LYP/6-311+G* Level

$E_{Tot.}$ (a.u.)			BE (eV)
MnB_9 (Singlet)	Mn (Quartet)	B_9 (Quartet)	
−1374.4008	−1150.89392	−223.27058	6.43
CoB_9 (Singlet)	Co (Quartet)	B_9 (Quartet)	
−1606.22716	−1382.70337	−223.26988	6.91
ZnB_{10} (Singlet)	Zn (Singlet)	B_{10} (Singlet)	
−2027.61764	−1779.35353	−248.08557	4.86

Magnetic Aromaticity. $NICS(1)_{zz}$[88−90] values (the out-of-plane ("zz") shielding tensor component of NICS(1)) for the singlet MB_n (n = 7 to 10) minima range from −102.9 in CuB_9^{2-} to −71.2 ppm in MnB_8^{3+} (Table 3) and document the aromatic character of the phMs (see Supporting Information, Tables S1 to S3 for $NICS(1)_{zz}$ of doublet, triplet, and quintuplet phM minima).

The π and radial double aromaticities[86] of VB_{10}^-, FeB9$^-$, and ZnB_9^- are demonstrated by the dissection of the NICS-$(1)_{zz}$ tensor into the individual canonical molecular orbital contributions (CMO-$NICS(1)_{zz}$)[91] (see Figure 1). The largely diatropic NICS tensors in VB_{10}^-(D_{10h}) originate from three π orbitals (−22.7 ppm from MOs 31, 32, and 33) and five radial MOs (−28.1 ppm from MOs 30, 34−37). The d AOs of the central V atom (except the vacant d_{z^2} AO) enhance the $NICS_{zz}$ tensor contribution through d-π and d-radial bonding interactions. Both π (−25.2 ppm from MOs 34, 37, and 38) and radial (−20.0 ppm from MOs 33, 35, and 36) aromaticities are observed in ZnB_9^-, although the magnitude of the $NICS(1)_{Radzz}$ tensor is reduced compared to the VB_{10}^-. The d AOs of the Zn atom do not participate in the π/radial bonding, and thus do not contribute to double aromaticity of ZnB_9^-;[86] the latter originates from the boron ring π and radial MOs (except MO 33, where the Zn 4s AO forms a radial bond with the boron ring). These contributions indicate the importance of the boron ring π and radial MOs in stabilizing the phMs.

The $NICS_{zz}$ grid of FeB_9^- (D_{9h}) (Figure 2, a), which shows a diatropic region above the molecular plane and a paratropic region outside of the boron ring, indicates aromatic character, and is consistent with the ring current model.[92] $NICS_{zz}$ grids of CCu_4^{2+},[93] SiB_8,[84] and CAl_5^+[23] and an induced magnetic field plot[80] of C_5^{2-}[94] reveal similar patterns. Dissecting the $NICS_{zz}$ grid into contributions from π and radial MOs (Figure 2, b and c, respectively) shows a similar cone-shaped diatropic region above the ring plane, and confirms the double aromaticity[86] in FeB_9^-. The NICS contributions from the remaining core and σ electrons (Figure 2d) are due to local shielding effects, as in Al_4^{2-},[95,96] and are negligible

(87) Allred, A. L.; Rochow, E. G. *J. Inorg. Nucl. Chem.* **1958**, *5*, 264–268.
(88) Steiner, E.; Fowler, P. W.; Jenneskens, L. W. *Angew. Chem., Int. Ed.* **2001**, *40*, 362–366.
(89) Chen, Z.; Wannere, C. S.; Corminboeuf, C.; Puchta, R.; Schleyer, P. v. R. *Chem. Rev.* **2005**, *105*, 3842–3888.
(90) Fallah-Bagher-Shaidaei, H.; Wannere, C. S.; Corminboeuf, C.; Puchta, R.; Schleyer, P. v. R. *Org. Lett.* **2006**, *8*, 863–866.
(91) Corminboeuf, C.; Heine, T.; Weber, J. *Phys. Chem. Chem. Phys.* **2003**, *5*, 246–251.
(92) Pople, J. A. *J. Chem. Phys.* **1956**, *24*, 1111–1112.
(93) Roy, D.; Corminboeuf, C.; Wannere, C.; King, R. B.; Schleyer, P. v. R. *Inorg. Chem.* **2006**, *45*, 8902–8906.
(94) Merino, G.; Mendez-Rojas, M. A.; Beltrán, H. I.; Corminboeuf, C.; Heine, T.; Vela, A. *J. Am. Chem. Soc.* **2004**, *126*, 16160–16169.
(95) Fowler, P. W.; Havenith, R. W. A.; Steiner, E. *Chem. Phys. Lett.* **2001**, *342*, 85–90.
(96) Fowler, P. W.; Havenith, R. W. A.; Steiner, E. *Chem. Phys. Lett.* **2002**, *359*, 530–536.

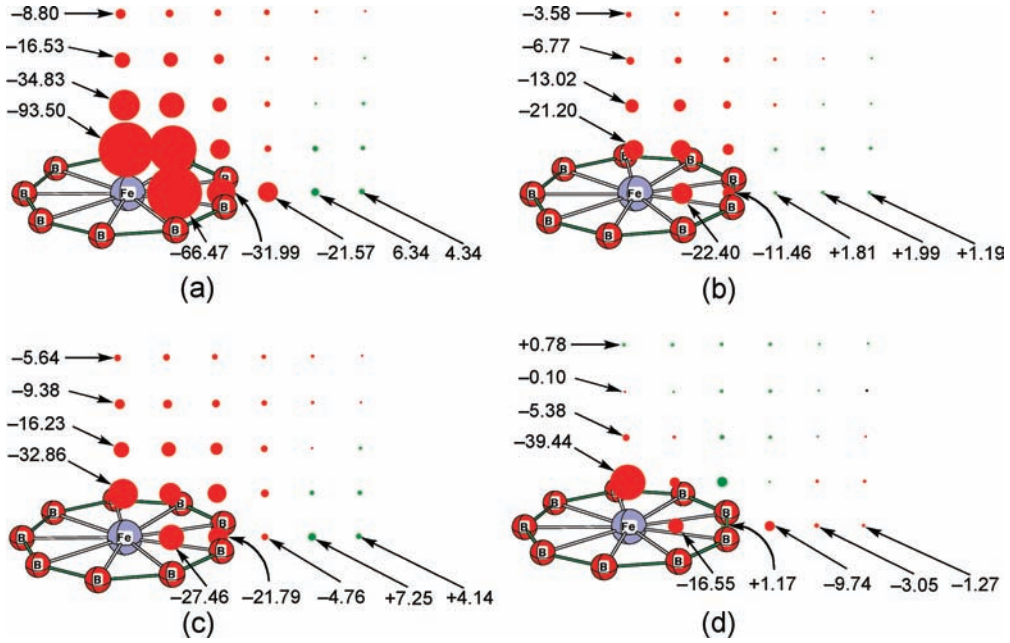

Figure 2. Grids of points of (a) total $NICS_{zz}$, (b) $NICS_{\pi zz}$, (c) $NICS_{Radzz}$, and (d) $NICS_{zz}$ sum from other MOs, including core and σ of D_{9h} FeB_9^-, at the GIAO/B3LYP/6-311G* level. Diatropic regions (in red) above the molecular plane, and paratropic regions (in green) document the double aromaticity.

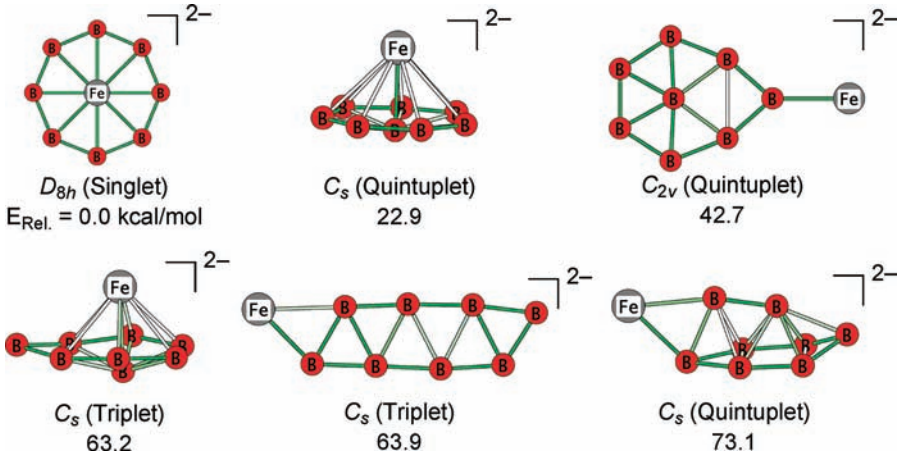

Figure 3. Optimized structures and relative energies (E_{Rel}, in kcal/mol at B3LYP/6-311+G*// B3LYP/6-311+G*) of the lowest energy FeB_8^{2-} minima from stochastic Kick searches.

(except when close to an atom, e.g., the −39.4 ppm point 1.0 Å away from Fe).

Effects of Electron Attachment/Detachment. Table 3 shows the number of π, radial, lone pair d AO, and σ electrons in the singlet phM minima. Although D_{8h} CoB_8^{3+} is a minimum with 6 π electrons, it has only 6 radial electrons (less than optimum in an 8MR). Four additional electrons occupy the degenerate radial bonds with one node (rad_1, similar to the MOs 35 and 36 in the D_{9h} FeB_9^-, Figure 1) and bond the peripheral ring more tightly. Additional radial bonds increase the magnitude of electron delocalization, and explain the significant increase in the $NICS(1)_{zz}$ of CoB_8^- compared to CoB_8^{3+}. Furthermore, the increased π bond character shortens the B−B bond distances from 1.602 Å (CoB_8^{3+}) to 1.559 Å (CoB_8^-). The Co−B separation decreases because of the contraction of the boron ring; however, the additional electrons have negligible effects on the Co−B bonding character, as indicated by the WBI_{M-B} (0.36 for both CoB_8^{3+} and CoB_8^-: see Table 2). This result reinforces the earlier observation that 6 π and 10 radial electron counts maximize the stability of the phMs.

The four additional electrons in D_{10h} CuB_{10}^- (compared to D_{10h} CuB_{10}^{3+}) occupy degenerate π MOs (similar to MOs 37 and 38 in D_{9h} ZnB_9^-, Figure 1). The increase in π bonding is evident from the B−B bond length contraction (1.577 Å in CuB_{10}^{3+}; 1.524 Å in CuB_{10}^-) as well as from the $NICS(1)_{zz}$ values (−100.5 in CuB_{10}^- and −81.1 ppm in CuB_{10}^{3+}). However, the degenerate HOMOs of the CuB_{10}^- have slight Cu−B antibonding character and decreases the WBI_{M-B} in CuB_{10}^- slightly to 0.10 from the 0.12 value in CuB_{10}^{3+}.

However, the two "extra" electrons in the D_{9h} MnB_9^{2-} dianion (vs D_{9h} MnB_9) occupy the lone pair d_{z^2} Mn AO (akin to MO 34 in FeB_9^-, Figure 1). This d_{z^2} MO lacks bonding character, hence the B−B bond lengths (1.526 Å in MnB_9 and 1.527 Å in MnB_9^{2-}, see Table 1) and the Mn−B separations (2.231 in MnB_9 and 2.232 Å in MnB_9^{2-}) are

essentially the same. Since the two added electrons are not delocalized, NICS(1)$_{zz}$ also is not changed significantly (MnB_9: −87.2 and MnB_9^{2-}: −90.6). These comparisons underscore the importance of 6 π and 10 radial electrons to maximize the stability of phMs. The effect of electron addition (or subtraction) is dominated by the bonding (or antibonding) character of the HOMO.

Potential Energy Surface Scan. The optimized minima and their relative energies are shown in Figure 3. The energy of D_{8h} FeB_8^{2-}, the global minimum, is 22.9 kcal/mol lower than that of the second best isomer. The central position of the Fe allows very efficient utilization of its d-orbitals in bonding in D_{8h} planar geometry. Our potential energy surface scan findings are also in agreement with Boldyrev's rule,[19,47,48] that the d-block elements, being more electropositive than B, prefer the ring center, rather than a peripheral position. Indeed, we found that the global CoB_8^- and FeB_9^- minima have D_{nh} symmetry.[68] Although related D_{nh} species (such as NiB_9^+ and CoB_9) are not global minima, they illustrate the broad extent of possible planar hypercoordination involving first row d-block metals, and invite experimental investigation, for example, by laser ablation/photoelectron spectroscopy.

4. Summary

A systematic computational survey reveals that many species composed of D_{nh} n-membered (n = 7 to 10) boron rings enclosing planar hypercoordinate first row transition metal atoms are at least local minima. With the exception of Co, the diameter of the B_7 ring is not large enough to accommodate first row d-block elements. The B_8 ring ligand only can enclose smaller d-block metals (Mn, Co, and Fe) in planar minima. The sizes of the B_9 cavity and the Ti, V, Cr, and Mn atoms match well, but the B_9 ring also can accept metals with smaller atomic radii. The B_{10} ring is too large to accommodate most of the first row d-block elements, except for Sc and Ti. Generally, both π and radial MOs bind the peripheral boron atoms to a central metal atom; the d AOs of the d-block metals also participate in d-π and d-radial bonding and help bind the metal atom to the boron ring ligand. The ionic bonding character between the metal and the boron ring increases for the late d-block metal species and helps to encapsulate the metal at the ring centers.

Acknowledgment. This work is supported by the 111 Project (B07012) in China and NSF Grant (CHE-0716718) in the U.S.A. Some computations were performed at the Research Computing Center at the University of Georgia.

Supporting Information Available: Total energies, zero-point energies, bond lengths, lowest vibrational frequencies, HOMO−LUMO gap, NICS(1)$_{zz}$, and number of the valence electrons of the doublet, triplet, and quintuplet minima, potential energy surface of D_{10h} NiB_{10}^{2+} along the trajectory of the lowest harmonic vibrational frequency, Cartesian coordinates of all of the minima, and the complete Gaussian03 reference 74. This material is available free of charge via the Internet at http://pubs.acs.org.